Anti-Dead-Zone Integral Sliding Control and Active Vibration Suppression of a Free-floating Space Robot with Elastic Base and Flexible Links

Xiaoqin Huang[1,2,✉] and Li Chen[2]

(1. College of Physics and Electronic Information Engineering, Minjiang University, Fuzhou 350108, China;
2. School of Mechanical Engineering and Automation, Fuzhou University, Fuzhou 350116, China)

Abstract: Under the conditions of joint torque output dead-zone and external disturbance, the trajectory tracking and vibration suppression for a free-floating space robot (FFSR) system with elastic base and flexible links were discussed. First, using the Lagrange equation of the second kind, the dynamic model of the system was derived. Second, utilizing singular perturbation theory, a slow subsystem describing the rigid motion and a fast subsystem corresponding to flexible vibration were obtained. For the slow subsystem, when the width of dead-zone is uncertain, a dead-zone pre-compensator was designed to eliminate the impact of joint torque output dead-zone, and an integral sliding mode neural network control was proposed. The integral sliding mode term can reduce the steady state error. For the fast subsystem, an optimal linear quadratic regulator (LQR) controller was adopted to damp out the vibration of the flexible links and elastic base simultaneously. Finally, computer simulations show the effectiveness of the compound control method.

Key words: space robot with flexible links; elastic base; dead-zone; proportional-integral sliding mode control; active vibration suppression

CLC number: TP 241 **Document code**: A **Article ID**: 1004-0579(2020)01-0120-09

Free-floating space robots (FFSRs) are complex, nonlinear and strong coupling dynamic systems, and they plays an indispensable role in space exploration. They can replace astronauts performing a variety of space tasks on orbit. Therefore, they have received extensive attention[1-3]. Ref. [4] explored the application of nonlinear model predictive control (NMPC) strategies in the redundant space robot, and the simulations showed its effectiveness. Ref. [5] studied the free-floating space manipulator system with the initial angular momentum not assumed to be zero and its influence on system behaviour.

The FFSR with flexible links is getting increasing attention because of its characteristics of light weight, long arm, heavy load, and more[6-8]. In order to complete space tasks with high precision, in addition to the trajectory tracking, vibration suppression must also be considered. Ref. [9] studied active damping strategies and relevant devices that could be used to reduce the structural vibrations of a space manipulator with flexible links during its in-orbit operations. Ref. [10] used the singular perturbation method to divide the space manipulator system with flexible links into slow and fast components, and simulation results showed that the link vibrations had been stabilized effectively.

In order to expand the working range of a FFSR on space stations, it is installed on a mobile

Received 2018-12-20
Supported by the National Natural Science Foundation of China (11372073, 11072061); Industrial Robot Basic Component Technology Research and Development Platform, Fujian, China (2014H21010011)
✉ Author for correspondence, lecturer, Ph. D.
E-mail: hxq582p@163.com
DOI: 10.15918/j.jbit1004-0579.18173

base which can move along the guide rails assembled by a truss. The system inevitably causes the elastic vibration of guide rail which would drive the vibration of the base in the operation process[11]. The tracking trajectory deviation is caused by the coupling relationship among rigid motion, base elasticity, and flexible vibration, which affects the control precision of the FFSR. Hence the base elasticity should be considered as a factor in the high-precision control of FFSR. Under the influence of base elasticity, Ref. [12] adopted a cascade control method to suppress the vibration of the elastic base and flexible joints of flexible-joint FFSR.

Futhermore, there is a dead-zone nonlinearity in the space manipulator actuator system, which is caused by the insensitivity of physical devices (such as sensors or drives, etc.) to some small signals. It gives rise to steady-state tracking error, oscillation of the limit cycle, and even control failure. Therefore, it is worthwhile to design a suitable dead-zone compensation method to improve the control accuracy. Ref. [13] took the space manipulator with dead-zone as the research object, and designed a recursive CMAC control method and a dead-zone pre-compensator to realize the trajectory tracking. Ref. [14] studied an adaptive backstepping control scheme and a dead-zone estimator for the robot manipulator with asymmetric dead-zone. However, neither of them considered the flexibility of the links and the base.

In light of the above research, under the joint torque output dead-zone and external disturbance, the trajectory tracking and vibration suppression for a FFSR with multiple flexible links and elastic base are discussed. Based on the singular perturbation theory, a slow subsystem describing the rigid motion and a fast subsystem corresponding to vibration are obtained. For the slow subsystem, a dead-zone pre-compensator is designed to eliminate the impact of joint torque output dead-zone, and an integral sliding mode neural network controller is proposed. For the fast subsystem, an optimal LQR controller is adopted to damp out the vibration of the flexible links and elastic base, which guarantees the stability and tracking accuracy. Numerical simulations of a FFSR system with an elastic base and two flexible links show the effectiveness of the proposed scheme.

1 Dynamics Modelling of a FFSR with Elastic Base and Multiple Flexible Links

The structure model of FFSR with an elastic base and n flexible links is shown in Fig. 1. The system consists of the free-floating base B_0 and the flexible links $B_i\ (i=1,2,\cdots,n)$. In order to simplify the operation, the elasticity of the guideway is simplified as a light spring to indicate the elasticity of the base. x' is the elastic displacement of the spring. The local coordinate $O_i x_i y_i$ of each fragment $B_i\ (i=0,1,\cdots,n)$ is established. O_0 coincides O_{c0}, which is the mass center of B_0. The rotary joint O_1 of B_1 is connected with B_0 by the light spring. $O_i\ (i=2,3,\cdots,n)$ is the rotational center of the revolute joint between B_{i-1} and B_i. The x_i-axis is collinear with $O_i O_{i+1}$ for $i=0,1,\cdots,n-1$, and the x_n-axis is tangent to B_n at O_n. The distance between O_1 and O_0 is l_0. The length of $B_i\ (i=1,2,\cdots,n)$ along the x_i-axis is l_i. The mass and moment of inertia about the centroid of the base are m_0 and J_0, respectively. A

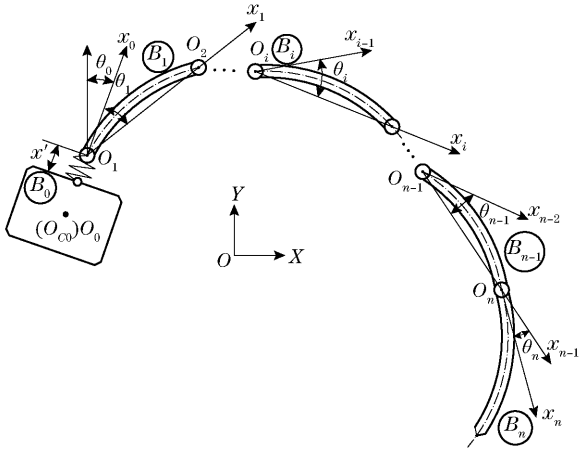

Fig. 1 FFSR system with elastic base and flexible links

translational inertial reference frame (O-XY) is established by taking the arbitracy point O of the space as the origin.

Assumption

① The spring is a massless spring;

② The spring can only stretch;

③ Elastic coefficient of the spring $k_{x'}$ is constant;

④ The initial displacement x' of the spring is zero.

The flexible links are slender and homogeneous. The bending deformation is mainly considered. The axial and shear deformation can be ignored, while transverse vibration is performed in the plane.

$(EI)_i$ is the flexural rigidity of link $B_i(i=1,2,\cdots,n)$, and ρ_i is the uniform density of the flexible link $B_i(i=1,2,\cdots,n)$. According to the assumed mode method[15], the flexible links can be regarded as Bernoulli-Euler beams. Then, their elastic deformations can be described as

$$w_i(x_i,t)=\sum_{j=1}^{\gamma_i}\varphi_{ij}(x_i)\delta_{ij}(t) \tag{1}$$

where $w_i(x_i,t)$ is the transverse elastic deformation of B_i at section $x_i(0\leqslant x_i\leqslant l_i)$. $\varphi_{ij}(x_i)$ is jth order modal function of link i. $\delta_{ij}(t)$ is the modal coordinate associated with $\varphi_{ij}(x_i)$. γ_i is the truncation of the flexible link $B_i(i=1,2,\cdots,n)$. $B_i(i=1,2,\cdots,n-1)$ and B_n are regarded as simply-supported beams and a cantilever beam, respectively. According to Ref. [16], their modal functions can be expressed.

According to a Lagrange equation of the second kind, the dynamic equation is obtained as

$$\boldsymbol{M}(\boldsymbol{\theta},\boldsymbol{\eta})\begin{bmatrix}\ddot{\boldsymbol{\theta}}\\ \ddot{\boldsymbol{\eta}}\end{bmatrix}+\boldsymbol{H}(\boldsymbol{\theta},\boldsymbol{\eta},\dot{\boldsymbol{\theta}},\dot{\boldsymbol{\eta}})\begin{bmatrix}\dot{\boldsymbol{\theta}}\\ \dot{\boldsymbol{\eta}}\end{bmatrix}+\begin{bmatrix}\boldsymbol{0}_{(n+1)\times 1}\\ \boldsymbol{K}_\eta\boldsymbol{\eta}\end{bmatrix}=\begin{bmatrix}\boldsymbol{\tau}\\ \boldsymbol{0}_{\left(\sum_{i=1}^{n}\gamma_i+1\right)\times 1}\end{bmatrix} \tag{2}$$

where $\boldsymbol{\theta}=[\theta_0\cdots\theta_i\cdots\theta_n]^{\mathrm{T}}\in\mathbf{R}^{n+1}$ is the generalized coordinate vector of the base and the multiple-link joints' relative angles, $\boldsymbol{\delta}=[\delta_{11}\cdots\delta_{1\gamma_1}\cdots\delta_{n\gamma_i}]^{\mathrm{T}}\in\mathbf{R}^{\sum_{i=1}^{n}\gamma_i}$ is the generalized coordinate vector of flexible modal coordinates, $\boldsymbol{\eta}=[\boldsymbol{\delta}^{\mathrm{T}}\quad x']^{\mathrm{T}}$, $\boldsymbol{M}(\boldsymbol{\theta},\boldsymbol{\eta})\in\mathbf{R}^{\left(n+2+\sum_{i=1}^{n}\gamma_i\right)\left(n+2+\sum_{i=1}^{n}\gamma_i\right)}$ is the symmetric positive inertia matrix, $\boldsymbol{H}(\boldsymbol{\theta},\boldsymbol{\eta},\dot{\boldsymbol{\theta}},\dot{\boldsymbol{\eta}})[\dot{\boldsymbol{\theta}}^{\mathrm{T}}\quad\dot{\boldsymbol{\eta}}^{\mathrm{T}}]^{\mathrm{T}}\in\mathbf{R}^{n+2+\sum_{i=1}^{n}\gamma_i}$ is the column vector containing the Coriolis and centrifugal forces, $\boldsymbol{K}_\eta=\mathrm{diag}\{\boldsymbol{K}_\delta,k_{x'}\}$, $\boldsymbol{K}_\delta=\mathrm{diag}(k_{11},\cdots,k_{n\gamma_i})\in\mathbf{R}^{\left(\sum_{i=1}^{n}\gamma_i\right)\left(\sum_{i=1}^{n}\gamma_i\right)}$ $\left(k_{ij}=(EI)_i\int_0^{l_i}(\varphi_{ij}'')^2\mathrm{d}x_i\right)$ are the stiffness matrix of the flexible links, and $\boldsymbol{\tau}=(\tau_0\cdots\tau_i\cdots\tau_n)^{\mathrm{T}}\in\mathbf{R}^{n+1}$ is the vector of the base and joint input torques.

2 Fast and Slow Subsystem Decomposition Based on Singular Perturbation

The dynamic system is decomposed into a slow subsystem representing rigid motion and a fast subsystem which expresses the elasticity of base and the vibration of flexible links. Eq. (2) with block matrices can be rewritten as

$$\begin{bmatrix}\boldsymbol{M}_{rr}&\boldsymbol{M}_{rf}\\ \boldsymbol{M}_{fr}&\boldsymbol{M}_{ff}\end{bmatrix}\begin{bmatrix}\ddot{\boldsymbol{\theta}}\\ \ddot{\boldsymbol{\eta}}\end{bmatrix}+\begin{bmatrix}\boldsymbol{H}_{rr}&\boldsymbol{H}_{rf}\\ \boldsymbol{H}_{fr}&\boldsymbol{H}_{ff}\end{bmatrix}\begin{bmatrix}\dot{\boldsymbol{\theta}}\\ \dot{\boldsymbol{\eta}}\end{bmatrix}+\begin{bmatrix}\boldsymbol{0}_{(n+1)\times 1}\\ \boldsymbol{K}_\eta\boldsymbol{\eta}\end{bmatrix}=\begin{bmatrix}\boldsymbol{\tau}\\ \boldsymbol{0}_{\left(\sum_{i=1}^{n}\gamma_i+1\right)\times 1}\end{bmatrix} \tag{3}$$

where $\boldsymbol{M}_{rr}\in\mathbf{R}^{(n+1)\times(n+1)}$, $\boldsymbol{M}_{ff}\in\mathbf{R}^{\left(\sum_{i=1}^{n}\gamma_i+1\right)\left(\sum_{i=1}^{n}\gamma_i+1\right)}$ and $\boldsymbol{M}_{rf}=\boldsymbol{M}_{fr}^{\mathrm{T}}\in\mathbf{R}^{(n+1)\times\left(\sum_{i=1}^{n}\gamma_i+1\right)}$ are the sub-matrices of $\boldsymbol{M}(\boldsymbol{\theta},\boldsymbol{\eta})$, $\boldsymbol{H}_{rr}\in\mathbf{R}^{(n+1)\times(n+1)}$, $\boldsymbol{H}_{rf}\in\mathbf{R}^{(n+1)\times\left(\sum_{i=1}^{n}\gamma_i+1\right)}$, $\boldsymbol{H}_{fr}\in\mathbf{R}^{\left(\sum_{i=1}^{n}\gamma_i+1\right)\times(n+1)}$, and $\boldsymbol{H}_{ff}\in\mathbf{R}^{(n+1)\times\left(\sum_{i=1}^{n}\gamma_i+1\right)}$ are the sub-matrices of $\boldsymbol{H}(\boldsymbol{\theta},\boldsymbol{\eta},\dot{\boldsymbol{\theta}},\dot{\boldsymbol{\eta}})$.

Since $\boldsymbol{M}$ is a symmetric, positive definite matrix, its inverse exists and can be written as

$$\boldsymbol{N}=\boldsymbol{M}^{-1}=\begin{bmatrix}\boldsymbol{M}_{rr}&\boldsymbol{M}_{rf}\\ \boldsymbol{M}_{fr}&\boldsymbol{M}_{ff}\end{bmatrix}^{-1}=\begin{bmatrix}\boldsymbol{N}_{rr}&\boldsymbol{N}_{rf}\\ \boldsymbol{N}_{fr}&\boldsymbol{N}_{ff}\end{bmatrix} \tag{4}$$

where

$$\boldsymbol{N}_{rr}=(\boldsymbol{M}_{rr}-\boldsymbol{M}_{rf}\boldsymbol{M}_{ff}^{-1}\boldsymbol{M}_{fr})^{-1}$$

$$\boldsymbol{N}_{rf}=-\boldsymbol{M}_{rr}^{-1}\boldsymbol{M}_{rf}(\boldsymbol{M}_{ff}-\boldsymbol{M}_{fr}\boldsymbol{M}_{rr}^{-1}\boldsymbol{M}_{rf})^{-1}$$

$$\boldsymbol{N}_{rf} = -\boldsymbol{M}_{ff}^{-1}\boldsymbol{M}_{fr}(\boldsymbol{M}_{rr} - \boldsymbol{M}_{rf}\boldsymbol{M}_{ff}^{-1}\boldsymbol{M}_{fr})^{-1}$$

$$\boldsymbol{N}_{ff} = (\boldsymbol{M}_{ff} - \boldsymbol{M}_{fr}\boldsymbol{M}_{rr}^{-1}\boldsymbol{M}_{rf})^{-1}$$

We define the singular perturbation scale factor $\varepsilon = 1/\sqrt{\min\{k_{11}, \cdots, k_{n\gamma_i}, k_{x'}\}}$, new state variables $\boldsymbol{z} = \boldsymbol{\eta}/\varepsilon^2$, and new matrix $\widetilde{\boldsymbol{K}} = \varepsilon^2\boldsymbol{K}_\eta$. When ε is small enough, the smallest element of $\boldsymbol{K}_\eta$ is sufficiently large. Thus, the singular perturbation model of the FFSR system with elastic base and flexible links is obtained as

$$\ddot{\boldsymbol{\theta}} = -(\boldsymbol{N}_{rr}\boldsymbol{H}_{rr} + \boldsymbol{N}_{rf}\boldsymbol{H}_{fr})\dot{\boldsymbol{\theta}} - (\boldsymbol{N}_{rr}\boldsymbol{H}_{rf} + \boldsymbol{N}_{rf}\boldsymbol{H}_{ff})\varepsilon^2\dot{\boldsymbol{z}} - \boldsymbol{N}_{rf}\widetilde{\boldsymbol{K}}\boldsymbol{z} + \boldsymbol{N}_{rr}\boldsymbol{\tau} \quad (5a)$$

$$\varepsilon^2\ddot{\boldsymbol{z}} = -(\boldsymbol{N}_{fr}\boldsymbol{H}_{rr} + \boldsymbol{N}_{ff}\boldsymbol{H}_{fr})\dot{\boldsymbol{\theta}} - (\boldsymbol{N}_{fr}\boldsymbol{H}_{rf} + \boldsymbol{N}_{ff}\boldsymbol{H}_{ff})\varepsilon^2\dot{\boldsymbol{z}} - \boldsymbol{N}_{ff}\widetilde{\boldsymbol{K}}\boldsymbol{z} + \boldsymbol{N}_{fr}\boldsymbol{\tau} \quad (5b)$$

Define the combination control law

$$\boldsymbol{\tau} = \bar{\boldsymbol{\tau}} + \boldsymbol{\tau}_f \quad (6)$$

where $\bar{\boldsymbol{\tau}}$ is to control the slow subsystem and $\boldsymbol{\tau}_f$ is to control the fast subsystem.

In order to obtain the slow subsystem, the singular perturbation model is evaluated with $\varepsilon = 0$, then the following equations are obtained

$$\ddot{\bar{\boldsymbol{\theta}}} = -(\bar{\boldsymbol{N}}_{rr}\bar{\boldsymbol{H}}_{rr} + \bar{\boldsymbol{N}}_{rf}\bar{\boldsymbol{H}}_{fr})\dot{\bar{\boldsymbol{\theta}}} - \bar{\boldsymbol{N}}_{rf}\widetilde{\bar{\boldsymbol{K}}}\bar{\boldsymbol{z}} + \bar{\boldsymbol{N}}_{rr}\bar{\boldsymbol{\tau}} \quad (7a)$$

$$0 = -(\bar{\boldsymbol{N}}_{fr}\bar{\boldsymbol{H}}_{rr} + \bar{\boldsymbol{N}}_{ff}\bar{\boldsymbol{H}}_{fr})\dot{\bar{\boldsymbol{\theta}}} - \bar{\boldsymbol{N}}_{ff}\widetilde{\bar{\boldsymbol{K}}}\bar{\boldsymbol{z}} + \bar{\boldsymbol{N}}_{fr}\bar{\boldsymbol{\tau}} \quad (7b)$$

where the matrix or variable with a crossed "$-$" means the corresponding slow variable component.

Then $\bar{\boldsymbol{z}}$ can be solved by Eq. (7b):

$$\bar{\boldsymbol{z}} = \widetilde{\bar{\boldsymbol{K}}}^{-1}\bar{\boldsymbol{N}}_{ff}^{-1}[-(\bar{\boldsymbol{N}}_{fr}\bar{\boldsymbol{H}}_{rr} + \bar{\boldsymbol{N}}_{ff}\bar{\boldsymbol{H}}_{fr})\dot{\bar{\boldsymbol{\theta}}} + \bar{\boldsymbol{N}}_{fr}\bar{\boldsymbol{\tau}}] \quad (8)$$

Substituting Eq. (8) into Eq. (5a), the slow subsystem is obtained as

$$\bar{\boldsymbol{M}}_{rr}\ddot{\bar{\boldsymbol{\theta}}} + \bar{\boldsymbol{H}}_{rr}\dot{\bar{\boldsymbol{\theta}}} = \bar{\boldsymbol{\tau}} \quad (9)$$

In order to obtain the fast subsystem, a fast variable time scale $\omega = t/\varepsilon$ is introduced, and boundary layer correction terms are defined as: $\boldsymbol{p}_1 = \boldsymbol{z} - \bar{\boldsymbol{z}}$, $\boldsymbol{p}_2 = \varepsilon\dot{\boldsymbol{z}}$. Eq. (5b) can be rewritten as

$$\frac{\mathrm{d}\boldsymbol{p}_1}{\mathrm{d}\omega} = \boldsymbol{p}_2 - \varepsilon\dot{\bar{\boldsymbol{z}}} \quad (10a)$$

$$\frac{\mathrm{d}\boldsymbol{p}_2}{\mathrm{d}\omega} = -(\boldsymbol{N}_{fr}\boldsymbol{H}_{rr} + \boldsymbol{N}_{ff}\boldsymbol{H}_{fr})\dot{\boldsymbol{\theta}} - (\boldsymbol{N}_{fr}\boldsymbol{H}_{rf} + \boldsymbol{N}_{ff}\boldsymbol{H}_{ff})\varepsilon\boldsymbol{p}_2 - \boldsymbol{N}_{ff}\widetilde{\boldsymbol{K}}(\boldsymbol{p}_1 + \bar{\boldsymbol{z}}) + \boldsymbol{N}_{fr}\boldsymbol{\tau} \quad (10b)$$

Setting $\varepsilon = 0$, thus the fast subsystem is

$$\frac{\mathrm{d}\boldsymbol{p}_1}{\mathrm{d}\omega} = \boldsymbol{p}_2 \quad (11a)$$

$$\frac{\mathrm{d}\boldsymbol{p}_2}{\mathrm{d}\omega} = -\bar{\boldsymbol{N}}_{ff}\widetilde{\bar{\boldsymbol{K}}}\boldsymbol{p}_1 + \bar{\boldsymbol{N}}_{fr}\boldsymbol{\tau}_f \quad (11b)$$

3 Combined Control Law Design

3.1 Dead-zone pre-compensator design

The joint torque output dead-zone is used to describe the system's insensitivity to small signals. When the signal enters the dead-zone, there would be considerable loss, which leads to the control deviation.

The adjustment of the base attitude and position of the space robot is usually carried out by a momentum wheel or a reaction jet thruster. While the joint hinges are driven by motors, there is a joint torque output dead-zone. Assuming that $\bar{\boldsymbol{\tau}}_p(t) = [\bar{\tau}_{p1} \quad \cdots \quad \bar{\tau}_{pn}]^{\mathrm{T}} \in \mathbf{R}^n$ is the dead-zone input and $\bar{\boldsymbol{\tau}}_r = [\bar{\tau}_1 \quad \cdots \quad \bar{\tau}_n]^{\mathrm{T}} = W(\bar{\boldsymbol{\tau}}_p)$ is the dead-zone output, then the dead-zone model is as follows[17].

$$\bar{\boldsymbol{\tau}}_r = \bar{\boldsymbol{\tau}}_p - \mathrm{sat}(\bar{\boldsymbol{\tau}}_p) \quad (12)$$

$$\mathrm{sat}_i(\bar{\boldsymbol{\tau}}_{pi}) = \begin{cases} d_{i+}, & \bar{\tau}_{pi} \geqslant d_{i+} \\ \bar{\tau}_{pi}, & -d_{i-} < \bar{\tau}_{pi} < d_{i+} \\ -d_{i-}, & \bar{\tau}_{pi} \leqslant -d_{i-} \end{cases}$$

where d_{i-} and d_{i+} are left and right breakpoints of dead-zone, respectively, which are positive and unknown but bounded.

Then, the width of dead-zone is $\boldsymbol{D} = [\boldsymbol{d}_+ \quad \boldsymbol{d}_-]^{\mathrm{T}} \in \mathbf{R}^{2n\times n}$, $\boldsymbol{d}_+ = \mathrm{diag}(d_{1+}, \cdots, d_{i+}, \cdots, d_{n+})$, $\boldsymbol{d}_- = \mathrm{diag}(d_{1-}, \cdots, d_{i-}, \cdots, d_{n-})$. There exists a normal number D_M, which makes $\|\boldsymbol{D}\| \leqslant D_M$.

In order to compensate the adverse effect of dead-zone, a dead-zone pre-compensator is designed, whose principle is shown in Fig. 2. After the torque $\bar{\boldsymbol{w}}_r$ passes through the dead-zone pre-compensator, the dead-zone input $\bar{\boldsymbol{\tau}}_p$ is obtained, and $\bar{\boldsymbol{\tau}}_r$ is final output torque after $\bar{\boldsymbol{\tau}}_p$ passes through dead-zone. At this time, $\bar{\boldsymbol{\tau}}_r$ has eliminated the influence of the dead-zone, so that $\bar{\boldsymbol{\tau}}_r$ is con-

sistent with $\overline{\boldsymbol{w}}_r$. The dead-zone width is unknown, and the estimation $\hat{\boldsymbol{D}} = [\hat{\boldsymbol{d}}_+ \quad \hat{\boldsymbol{d}}_-]^{\mathrm{T}}$ is used to offset the dead-zone.

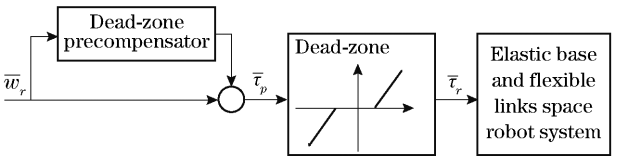

Fig. 2 Adaptive dead-zone compensation principle

Before passing through the dead-zone, $\overline{\boldsymbol{w}}_r$ is compensated by the dead-zone pre-compensator[18]

$$\overline{\boldsymbol{\tau}}_p = \overline{\boldsymbol{w}}_r + \hat{\boldsymbol{D}}^{\mathrm{T}}\overline{\boldsymbol{\mu}} \tag{13}$$

where $\overline{\boldsymbol{\mu}} = [\mu_1, \cdots \mu_n, (\mu_1 - 1), \cdots, (\mu_n - 1)]^{\mathrm{T}}$, $\mu_i = 1(\overline{w}_{ri} \geqslant 0)$ or $\mu_i = 0(\overline{w}_{ri} < 0)$.

Then $\overline{\boldsymbol{\tau}}_r$ can be derived as follows.[17]

$$\overline{\boldsymbol{\tau}}_r = \overline{\boldsymbol{w}}_r + \hat{\boldsymbol{D}}^{\mathrm{T}}\overline{\boldsymbol{\mu}} - \mathrm{sat}(\overline{\boldsymbol{w}}_r + \hat{\boldsymbol{D}}^{\mathrm{T}}\overline{\boldsymbol{\mu}}) = \overline{\boldsymbol{w}}_r - \widetilde{\boldsymbol{D}}^{\mathrm{T}}\overline{\boldsymbol{\mu}} + \widetilde{\boldsymbol{D}}^{\mathrm{T}}\boldsymbol{\chi} \tag{14}$$

where $\widetilde{\boldsymbol{D}} = \boldsymbol{D} - \hat{\boldsymbol{D}} = [\widetilde{\boldsymbol{d}}_+ \quad \widetilde{\boldsymbol{d}}_-]^{\mathrm{T}} \in \mathbf{R}^{2n \times n}$ is the matrix of dead-zone width estimation errors, and the modeling mismatch $\boldsymbol{\chi}$ satisfies the bound $\| \boldsymbol{\chi} \| \leqslant \sqrt{n}$[17].

3.2 Design the slow subsystem controller

While there exists the external disturbance $\boldsymbol{\tau}_d$, the slow subsystem can be written as

$$\overline{\boldsymbol{M}}_{rr}\ddot{\boldsymbol{\theta}} + \overline{\boldsymbol{H}}_{rr}\dot{\boldsymbol{\theta}} + \boldsymbol{\tau}_d = \overline{\boldsymbol{\tau}} \tag{15}$$

where $\overline{\boldsymbol{\tau}} = [\overline{\boldsymbol{\tau}}_0 \quad \overline{\boldsymbol{\tau}}_r^{\mathrm{T}}]^{\mathrm{T}} \in \mathbf{R}^{n+1}$.

We define the system tracking error

$$\boldsymbol{e} = \boldsymbol{\theta}_d - \boldsymbol{\theta} \tag{16}$$

where $\boldsymbol{\theta}_d = [\theta_{0d} \cdots \theta_{id} \cdots \theta_{nd}]^{\mathrm{T}}$ is the desired trajectory of rigid motion.

We define the filter trajectory error

$$\boldsymbol{s} = \boldsymbol{\Lambda}\boldsymbol{e} + \dot{\boldsymbol{e}} \tag{17}$$

where $\boldsymbol{\Lambda} \in \mathbf{R}^{(n+1)\times(n+1)}$ is a symmetric and positive definite constant matrix.

The slow subsystem Eq. (15) can be expressed as a form of error equation about $\boldsymbol{s}$

$$\overline{\boldsymbol{M}}_{rr}\dot{\boldsymbol{s}} = \overline{\boldsymbol{f}} - \overline{\boldsymbol{H}}_{rr}\boldsymbol{s} - \overline{\boldsymbol{\tau}} \tag{18}$$

where $\boldsymbol{q}_r = \boldsymbol{\Lambda}\boldsymbol{e} + \dot{\boldsymbol{\theta}}_d$ is the auxiliary reference output vector for the slow subsystem. $\overline{\boldsymbol{f}} = \overline{\boldsymbol{M}}_{rr}\dot{\boldsymbol{q}}_r + \overline{\boldsymbol{H}}_{rr}\boldsymbol{q}_r + \boldsymbol{\tau}_d$ is the sum of model uncertainty and external disturbance.

Because of the change of load and fuel consumption, the parameters of the dynamic model of the FFSR system are uncertain. In addition, space manipulators are inevitably affected by solar wind, cosmic rays and other external disturbance factors. For this reason, a Gaussian radial neural network is used to approximate $\overline{\boldsymbol{f}}$. This neural network is a three-layer forward neural network, which is based on the superposition of local approximation. Its advantage is that it has excellent approximation ability for strong nonlinear, fast convergence, and can avoid local minima.

Assuming $\overline{\boldsymbol{f}}_e$ is an approximation of $\overline{\boldsymbol{f}}$

$$\overline{\boldsymbol{f}}_e = \hat{\boldsymbol{W}}^{\mathrm{T}}\boldsymbol{\Phi} \tag{19}$$

where $\hat{\boldsymbol{W}}^{\mathrm{T}} = [w_{ij}]\,(i = 1, 2, \cdots, n; j = 1, 2, \cdots, h)$ is the network weight matrix. $\boldsymbol{\Phi}(\sigma) = [\Phi_1(\sigma), \cdots, \Phi_h(\sigma)]^{\mathrm{T}}$ is the basis function column vector. h is the number of the basis function center points. $\boldsymbol{\sigma} = [\boldsymbol{e}^{\mathrm{T}} \quad \dot{\boldsymbol{e}}^{\mathrm{T}}]^{\mathrm{T}}$ is the neural network input. The element of $\boldsymbol{\Phi}(\boldsymbol{\sigma})$ is the Gaussian function, which can be represented as

$$\Phi_j(\sigma) = \exp(-\| \sigma - c_j \|^2 / b_j^2) \tag{20}$$

where c_j is the center of the jth basis function, and b_j is the width of the corresponding basis function.

The optimal approximation of $\overline{\boldsymbol{f}}$ is

$$\overline{\boldsymbol{f}} = \overline{\boldsymbol{f}}^* = \boldsymbol{W}^{*\mathrm{T}}\boldsymbol{\Phi} + \psi \tag{21}$$

where $\boldsymbol{W}^*$ is the optimal value, ψ is the optimal approximation error, and $\| \psi \| \leqslant \alpha$.

The control law is designed for the slow subsystem

$$\overline{\boldsymbol{w}} = \overline{\boldsymbol{f}}_e + \boldsymbol{K}_1\boldsymbol{s} + \boldsymbol{K}_2 \int \boldsymbol{s}\,\mathrm{d}t + \alpha\boldsymbol{s} / \| \boldsymbol{s} \| \tag{22}$$

where $\overline{\boldsymbol{w}} = [\overline{\boldsymbol{\tau}}_0 \quad \overline{\boldsymbol{w}}_r^{\mathrm{T}}]^{\mathrm{T}}$; $\boldsymbol{K}_1$, $\boldsymbol{K}_2$ and $\boldsymbol{K}_s$ are positive constant matrices, respectively.

Eq. (22) is substituted into Eq. (18), thus it can be rewritten as

$$\overline{\boldsymbol{M}}_{rr}\dot{\boldsymbol{s}} = -\boldsymbol{K}_1\boldsymbol{s} - \boldsymbol{K}_2 \int \boldsymbol{s}\,\mathrm{d}t - \alpha \frac{\boldsymbol{s}}{\| \boldsymbol{s} \|} + \overline{\boldsymbol{f}}^* - \overline{\boldsymbol{f}}_e - \overline{\boldsymbol{H}}_{rr}\boldsymbol{s} - \begin{bmatrix} 0 \\ \widetilde{\boldsymbol{D}}^{\mathrm{T}}\boldsymbol{\chi} - \widetilde{\boldsymbol{D}}^{\mathrm{T}}\overline{\boldsymbol{\mu}} \end{bmatrix} \tag{23}$$

Theorem For a slow subsystem of the FF-SR with an elastic base and flexible links given by Eq. (15), $\boldsymbol{s}$ is eventually consistent bounded, i. e. , the tracking error $\boldsymbol{e}$ converges to zero in an arbitrary small neighborhood if the control law is given by Eq. (23) and the parameter adaptation laws are given by

$$\dot{\hat{\boldsymbol{D}}} = -\dot{\widetilde{\boldsymbol{D}}} = \boldsymbol{\Xi}\overline{\boldsymbol{\mu}}\boldsymbol{s}_r^{\mathrm{T}} - \xi\boldsymbol{\Xi}\hat{D}\,\|\,\boldsymbol{s}_r\,\| \tag{24}$$

$$\dot{\hat{\boldsymbol{W}}} = -\dot{\widetilde{\boldsymbol{W}}} = \boldsymbol{\kappa}\boldsymbol{\Phi}\boldsymbol{s}^{\mathrm{T}} \tag{25}$$

where $\boldsymbol{\kappa} \in \mathbf{R}^{h\times h}$, $\widetilde{\boldsymbol{W}} = \boldsymbol{W}^{*} - \hat{\boldsymbol{W}}$, $\boldsymbol{\Xi} \in \mathbf{R}^{2n\times 2n}$, $\xi > 0$.

Proof Constructing the following Lyapunov function

$$L = \frac{1}{2}\boldsymbol{s}^{\mathrm{T}}\overline{\boldsymbol{M}}_{rr}\boldsymbol{s} + \frac{1}{2}\mathrm{tr}(\widetilde{\boldsymbol{W}}^{\mathrm{T}}\boldsymbol{\kappa}^{-1}\widetilde{\boldsymbol{W}}) + \frac{1}{2}\left(\int \boldsymbol{s}\mathrm{d}t\right)^{\mathrm{T}}\boldsymbol{K}_2\left(\int \boldsymbol{s}\mathrm{d}t\right) + \frac{1}{2}\mathrm{tr}(\widetilde{\boldsymbol{D}}^{\mathrm{T}}\boldsymbol{\Xi}^{-1}\widetilde{\boldsymbol{D}}) \tag{26}$$

Taking the first derivative of L with respect to time t

$$\dot{L} = \boldsymbol{s}^{\mathrm{T}}\overline{\boldsymbol{M}}_{rr}\dot{\boldsymbol{s}} + \frac{1}{2}\boldsymbol{s}^{\mathrm{T}}\dot{\overline{\boldsymbol{M}}}_{rr}\boldsymbol{s} + \boldsymbol{K}_2\boldsymbol{s}^{\mathrm{T}}\left(\int_0^t \boldsymbol{s}\mathrm{d}t\right) - \mathrm{tr}(\widetilde{\boldsymbol{W}}^{\mathrm{T}}\boldsymbol{\kappa}^{-1}\dot{\hat{\boldsymbol{W}}}) - \mathrm{tr}(\widetilde{\boldsymbol{D}}^{\mathrm{T}}\boldsymbol{\Xi}^{-1}\dot{\hat{\boldsymbol{D}}}) \tag{27}$$

Substituting from Eqs. (23) – (25) yields

$$\dot{L} = \boldsymbol{s}^{\mathrm{T}}\left\{-\boldsymbol{K}_1\boldsymbol{s} - \boldsymbol{K}_2\int \boldsymbol{s}\mathrm{d}t - \alpha\frac{\boldsymbol{s}}{\|\,\boldsymbol{s}\,\|} + \widetilde{\boldsymbol{W}}^{\mathrm{T}}\boldsymbol{\Phi} + \psi - \begin{bmatrix} 0 \\ \widehat{\boldsymbol{D}}^{\mathrm{T}}\boldsymbol{\chi} - \widetilde{\boldsymbol{D}}^{\mathrm{T}}\overline{\boldsymbol{\mu}} \end{bmatrix}\right\} + \boldsymbol{K}_2\boldsymbol{s}^{\mathrm{T}}\left(\int_0^t \boldsymbol{s}\mathrm{d}t\right) + \frac{1}{2}\boldsymbol{s}^{\mathrm{T}}(\dot{\overline{\boldsymbol{M}}}_{rr} - 2\overline{\boldsymbol{H}}_{rr})\boldsymbol{s} - \mathrm{tr}(\widetilde{\boldsymbol{W}}^{\mathrm{T}}\boldsymbol{\Phi}\boldsymbol{s}^{\mathrm{T}}) - \mathrm{tr}[\widetilde{\boldsymbol{D}}^{\mathrm{T}}(\overline{\boldsymbol{\mu}}\boldsymbol{s}_r^{\mathrm{T}} - \xi\hat{\boldsymbol{D}}\,\|\,\boldsymbol{s}_r\,\|)] \tag{28}$$

Since $\overline{\boldsymbol{H}}_{rr}$ and $\dot{\overline{\boldsymbol{M}}}_{rr}$ meet the characteristic of skew symmetry: $\frac{1}{2}\boldsymbol{s}^{\mathrm{T}}\dot{\overline{\boldsymbol{M}}}_{rr}\boldsymbol{s} = \boldsymbol{s}^{\mathrm{T}}\overline{\boldsymbol{H}}_{rr}\boldsymbol{s}$, Eq. (28) can be rewritten as

$$\dot{L} = -\boldsymbol{s}^{\mathrm{T}}\boldsymbol{K}_1\boldsymbol{s} + \boldsymbol{s}^{\mathrm{T}}\left(\psi - \alpha\frac{\boldsymbol{s}}{\|\,\boldsymbol{s}\,\|}\right) - \boldsymbol{s}^{\mathrm{T}}\begin{bmatrix} 0 \\ \widetilde{\boldsymbol{D}}^{\mathrm{T}}\boldsymbol{\chi} \end{bmatrix} + \mathrm{tr}[\widetilde{\boldsymbol{D}}^{\mathrm{T}}\xi(\boldsymbol{D} - \widetilde{\boldsymbol{D}})\,\|\,\boldsymbol{s}_r\,\|\,] \tag{29}$$

Note that $\|\,\psi\,\| \leqslant \alpha$, $\|\,\boldsymbol{\chi}\,\| \leqslant \sqrt{n}$, $\|\,\boldsymbol{D}\,\| \leqslant M$, $\|\,\boldsymbol{s}_r\,\| \leqslant \|\,\boldsymbol{s}\,\|$:

$$\dot{L} \leqslant -k_{\min}\|\,\boldsymbol{s}\,\|^2 + \sqrt{n}\,\|\,\widetilde{\boldsymbol{D}}\,\|\,\|\,\boldsymbol{s}\,\| + \xi D_M\|\,\widetilde{\boldsymbol{D}}\,\|\,\|\,\boldsymbol{s}\,\| - \xi\,\|\,\widetilde{\boldsymbol{D}}\,\|^2\|\,\boldsymbol{s}\,\| \tag{30}$$

where $k_{\min} = \lambda_{\min}(\boldsymbol{K}_1)$ is the minimum singular value of matrix $\boldsymbol{K}_1$.

Therefore

$$\dot{L} \leqslant -\|\,\boldsymbol{s}\,\|(k_{\min}\|\,\boldsymbol{s}\,\| - \beta\|\,\widetilde{\boldsymbol{D}}\,\| + \xi\,\|\,\widetilde{\boldsymbol{D}}\,\|^2) \tag{31}$$

where $\beta \equiv \sqrt{n} + \xi D_M$.

In order to meet the condition that $\dot{L}$ is negative, so long as either $\|\,\boldsymbol{s}\,\| > \frac{\beta^2}{4k_{\min}\xi}$ or $\|\,\widetilde{\boldsymbol{D}}\,\| > \frac{\beta}{\xi}$. Therefore $L > 0$, $\dot{L} \leqslant 0$. Hence, $\dot{L}$ is negative outside the compact set $\left(\|\,\boldsymbol{s}\,\| < \frac{\beta^2}{4k_{\min}\xi}\right.$ or $\left.\|\,\widetilde{\boldsymbol{D}}\,\| < \frac{\beta}{\xi}\right)$, where $\|\,\boldsymbol{s}\,\|$ and $\|\,\widetilde{\boldsymbol{D}}\,\|$ decrease within the region. For the compact set within the region around the origin, according to the expansion of the Lyapunov theory, apparently, $\|\,\boldsymbol{s}\,\|$ and $\|\,\widetilde{\boldsymbol{D}}\,\|$ are uniformly ultimately bounded (UUB). Therefore, $\boldsymbol{s}(t)$ and $\hat{\boldsymbol{D}}(t)$ are UUB, i. e. , $\boldsymbol{e}$ converges to zero in an arbitrary small neighborhood.

3.3 Linear quadratic controller of fast subsystem

Based on the linear quadratic regulator, the control scheme for the fast subsystem is designed to suppress the vibration of the elastic base and the flexible links actively at the same time.

Setting $\boldsymbol{\zeta} = [\,\boldsymbol{p}_1^{\mathrm{T}} \quad \boldsymbol{p}_2^{\mathrm{T}}\,]^{\mathrm{T}}$, the fast subsystem Eq. (11) is expressed as a state equation

$$\dot{\boldsymbol{\zeta}} = \boldsymbol{A}\boldsymbol{\zeta} + \boldsymbol{Y}\boldsymbol{\tau}_f \tag{32}$$

where

$$\boldsymbol{A} = \begin{bmatrix} \boldsymbol{0}_{(\sum_{i=1}^{n}\gamma_i+1)\times(\sum_{i=1}^{n}\gamma_i+1)} & \boldsymbol{I}_{(\sum_{i=1}^{n}\gamma_i+1)(\sum_{i=1}^{n}\gamma_i+1)} \\ -\overline{\boldsymbol{N}}_{ff}\widehat{\boldsymbol{K}} & \boldsymbol{0}_{(\sum_{i=1}^{n}\gamma_i+1)\times(\sum_{i=1}^{n}\gamma_i+1)} \end{bmatrix}$$

$$\boldsymbol{Y} = \begin{bmatrix} \boldsymbol{0}_{(\sum_{i=1}^{n}\gamma_i+1)\times(n+1)} \\ \overline{\boldsymbol{N}}_{fr} \end{bmatrix}.$$

As shown in Eq. (32), the fast subsystem is a linear system, and the system state variable $\boldsymbol{\zeta}$ can be adjusted to zero by the optimal control

method, so that the base elasticity and the multiple links flexible vibrations can be suppressed. For a linear system, if the performance index function is defined as an integral quadratic function of the state variables and control variables and the control quantity $\boldsymbol{\tau}_f$ is obtained when the function is minimum, then the system can obtain the optimal performance.

The linear quadratic optimal performance index function is introduced as

$$\boldsymbol{Z}=\frac{1}{2}\int_0^{\infty}(\boldsymbol{\zeta}^{\mathrm{T}}\boldsymbol{Q}\boldsymbol{\zeta}+\boldsymbol{\tau}_f^{\mathrm{T}}\boldsymbol{R}\boldsymbol{\tau}_f)\,\mathrm{d}t \tag{33}$$

where $\boldsymbol{Q}\in\mathbf{R}^{(\sum_{i=1}^{n}2\gamma_i+2)\times(\sum_{i=1}^{n}2\gamma_i+2)}$ is a semi-definite weighted symmetric matrix, and $\boldsymbol{R}\in\mathbf{R}^{(n+1)\times(n+1)}$ is a positive definite weighted symmetric matrix.

By the linear quadratic optimal control theory, in order to minimize $\boldsymbol{Z}$, the controller should be designed as

$$\boldsymbol{\tau}_f=-\boldsymbol{R}^{-1}\boldsymbol{B}^{\mathrm{T}}\boldsymbol{P}\boldsymbol{\zeta} \tag{34}$$

where $\boldsymbol{P}$ satisfies the following Riccati algebraic equation

$$\boldsymbol{P}\boldsymbol{A}+\boldsymbol{A}^{\mathrm{T}}\boldsymbol{P}-\boldsymbol{P}\boldsymbol{B}\boldsymbol{R}^{-1}\boldsymbol{B}^{\mathrm{T}}\boldsymbol{P}+\boldsymbol{Q}=0 \tag{35}$$

4 Simulation Examples

Taking the model of a FFSR system with elastic base and two flexible links shown in Fig. 3 as an example, numerical simulations are carried out.

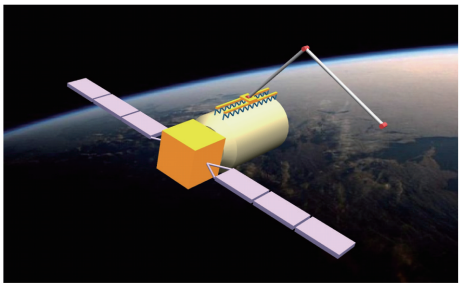

Fig. 3 FFSR system with elastic base and two flexible links

The system inertia and structural parameters are: $l_0=l_1=1.5$ m, $l_2=1.0$ m, $m_0=40$ kg, $J_0=34.17$ kg·m^2, $\rho_1=3.5$ kg/m, $\rho_2=1.1$ kg/m, $(EI)_1=50$ N·m^2, $(EI)_2=50$ N·m^2, $k_{x'}=500$ N/m.

The large amplitude vibration is mainly composed of the first few modes, so the truncation of flexible links is chosen as $\gamma_1=\gamma_2=2$. The external disturbance of the system is taken as

$$\boldsymbol{\tau}_d(t)=2.5\times$$
$$[\cos(\pi t/6)-\sin(\pi t/6)\quad\cos(\pi t/6)\quad\sin(\pi t/6)]^{\mathrm{T}}$$

The dead-zone widths are estimated as

$$\hat{\boldsymbol{d}}_+=\mathrm{diag}(10,10),\ \hat{\boldsymbol{d}}_-=\mathrm{diag}(5,5).$$

The desired angles $\boldsymbol{\theta}_d$ of the base and two flexible links respectively are: $\theta_{0\mathrm{d}}=-1$ rad, $\theta_{1\mathrm{d}}=0$ rad, $\theta_{2\mathrm{d}}=1$ rad. The initial angles are taken as: $\theta_0(0)=-1.2$ rad, $\theta_1(0)=-0.3$ rad, $\theta_2(0)=1.2$ rad. The initial displacement of the base spring is $x'(0)=0$. Simulation time is given by $t=50$ s.

Under the conditions of dead-zone and external disturbance, the integral sliding mode neural network control scheme is adopted for the FFSR with flexible links and an elastic base. Fig. 4 shows the actual trajectory (solid line) and the desired trajectory (dashed line) of base and two links. Fig. 5 shows the elastic vibration of the base, in which the elastic displacement is 0.018 m at 0.3 s and then decays to zero after 35 s. Figs. 6–7 show the first and second order modal of the two flexible links. The first order mode of the link B_1 attenuates from 0.366 m in the initial 1.0 s to zero after 45 s, while the second order mode of the link B_1 attenuates from 0.032 m in the initial 0.1 s to zero after 30 s. The first order mode of the link B_2 attenuates from 0.215 m in the initial 1.1 s to zero after 45 s, while the second order mode of the link B_2 attenuates from 0.045 m in the initial 0.2 s to zero after 20 s. From these simulation results, it can be seen that the actual trajectory of the base and the two joints can track the desired trajectory well and the

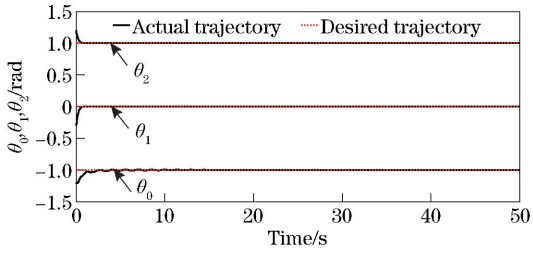

Fig. 4 Trajectory tracking of the base's attitude and the two links' joints

vibrations of the base and two flexible links are suppressed.

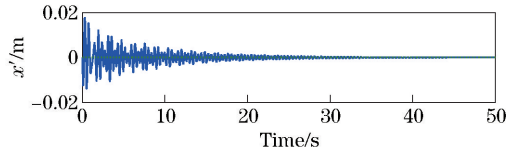

Fig. 5 Elastic displacement of the base

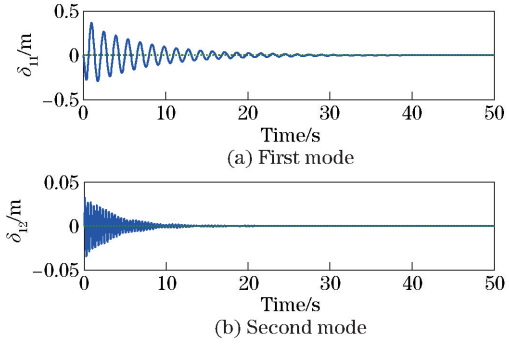

Fig. 6 Mode of flexible link B_1

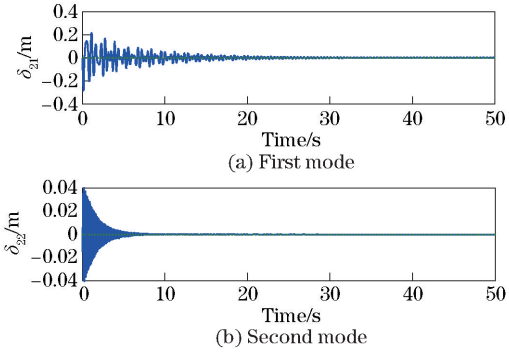

Fig. 7 Mode of flexible link B_2

In order to illustrate the effectiveness of the vibration suppression method, Figs. 8 – 9 show the first and second order modal of the two flexible links when $\boldsymbol{\tau}_f$ is closed. It can be seen from these figures, the first-order mode of the link B_1 vibrates is about ±0.08 m after 25 s, while the second-order mode of the link B_1 vibrates is about ±0.004 m after 10 s. The first-order mode of the link B_2 vibrates is about ±0.06 m after 10 s, while the second-order mode of the link B_2 vibrates is about ±0.005 m after 25 s. Fig. 10 simulates the base elastic displacement when $\boldsymbol{\tau}_f$ is closed. It can be seen that the base always vibrates between ±0.004 m. All the above can not suppress the vibration; thus, the effectiveness of the vibration suppression scheme is verified.

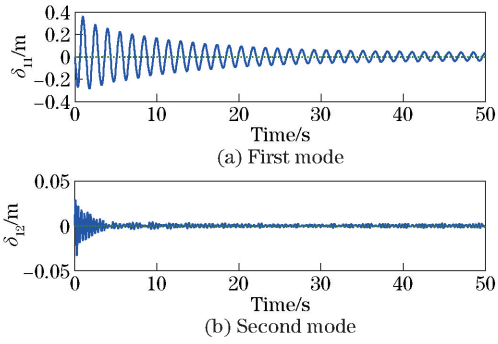

Fig. 8 Mode of flexible link B_1 (close $\boldsymbol{\tau}_f$)

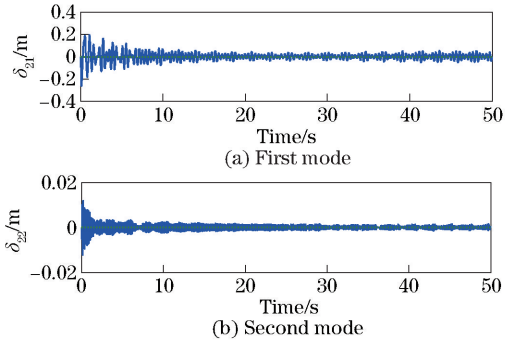

Fig. 9 Mode of flexible link B_2 (close $\boldsymbol{\tau}_f$)

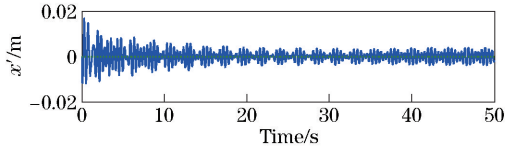

Fig. 10 Elastic displacement of the base (close $\boldsymbol{\tau}_f$)

For the sake of showing the effectiveness of the dead-zone pre-compensator, the trajectory tracking error of closing it is shown in Fig. 11. It can be seen clearly that the error of two joints is always unable to converge. Because of the multiple coupling relationship, there is a tracking error between the desired trajectory and the actual trajectory of the base angle, although there exists no dead-zone in it.

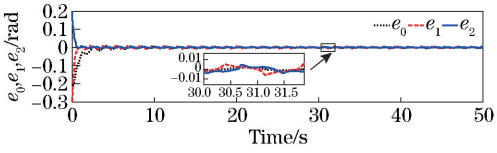

Fig. 11 Tracking error (off dead-zone compensation)

5 Conclusion

Considering the multiple coupling among rigid motion, base elasticity and flexible vibration,

the dynamic model of the FFSR system is derived. Based on the singular perturbation method, in the case of dead-zone and external disturbance, an integral sliding mode neural network control law of the slow subsystem and an optimal LQR controller of the fast subsystem are designed. A dead-zone pre-compensator is proposed to eliminate the impact of dead-zone, and the integral sliding mode term can reduce the steady-state error. The neural network can approximate the uncertainty of the dynamic equation and external disturbance. The simulation results show that the scheme can meet the control requirements.

References:

[1] Kumar N, Panwar V, Borm J H, et al. Adaptive neural controller for space robot system with an attitude controlled base[J]. Neural Computing and Applications, 2013, 23(7): 2333 –2340.

[2] Yoshida K. Engineering test satellite VII flight experiments for space robot dynamics and control: Theories on laboratory test beds ten years ago, now in orbit [J]. International Journal of Robotics Research, 2003, 22(5): 321 –335.

[3] Flores-Abad A, Ma O, Pham K, et al. A review of space robotics technologies for on-orbit servicing [J]. Progress in Aerospace Sciences, 2014, 68(8): 1 –26.

[4] Wang M M, Luo J J, Walter U. A non-linear model predictive controller with obstacle avoidance for a space robot [J]. Advances in Space Research, 2016, 57(8): 1737 –1746.

[5] Nanos K, Papadopoulos E. On the use of free-floating space robots in the presence of angular momentum [J]. Intelligent Service Robotics, 2011, 4(1): 3 –15.

[6] Hu J C, Wang T S. An o(n) complexity recursive algorithm for multi-flexible-body dynamics based on absolute nodal coordinate formulation[J]. International Journal for Numerical Methods in Engineering, 2017, 110(11): 1049 –1068.

[7] Liang L, Zhang D G, Guo Y B. Dynamic modeling and analysis of a rotating flexible beam with smart ACLD treatment[J]. Composites Part B: Engineering, 2017, 131: 221 –236.

[8] Singla A, Tewari A, Dasgupta B. Command shaped closed-loop control of flexible robotic manipulators [J]. Journal of Vibration Engineering & Technologies, 2016, 4(2): 97 –110.

[9] Sabatini M, Gasbarri P, Monti R, et al. Vibration control of a flexible space manipulator during on orbit operations [J]. Acta Astronautica, 2012, 73 (2): 109 –121.

[10] Yu X Y, Chen L. Singular perturbation adaptive control and vibration suppression of free-flying flexible space manipulators[J]. Proceedings of the Institution of Mechanical Engineers, Part C: Journal of Mechanical Engineering Science, 2015, 229 (11): 1989 –1997.

[11] Evans L. Canadian space robotics on board the international space[C]//2005 CCToMM Symposium on Mechanism, Machines, and Mechatronics, Canadian Space Agency, Montreal, Canada, 2005: 26 –27.

[12] Liang Jie, Chen Li. Robust adaptive sliding mode Control and dual vibration suppression in flexible joint manipulator of space station with elastic foundation[J]. Manned Spaceflight, 2016, 22(6): 788 –796. (in Chinese)

[13] Huang Xiaoqin, Chen Li. Anti-dead-zones and friction control of space robots with recurrent CMAC [J]. China Mechanical Engineering, 2018, 29(2): 211 –217. (in Chinese)

[14] Jeong Y C, Seong I H, Jang M L. Adaptive fuzzy dynamic surface sliding mode position control for a robot manipulator with friction and deadzone[J]. Mathematical Problems in Engineering, 2013, 2013 (4): 1 –15.

[15] Luca A D. Closed-form dynamic model of planar multilink lightweight robots[J]. IEEE Transactions on Systems, Man, and Cybernetics, 1991, 21(4): 826 –839.

[16] Liu Y Z, Chen L Q, Chen W L. Vibration mechanics [M]. 2nd ed. Beijing: Higher Education Press, 2011:130 –134.

[17] Lewis F L, Tim W K, Wang L Z, et al. Deadzone compensation in motion control systems using adaptive fuzzy logic control[J]. IEEE Transactions on Control Systems Technology, 1999, 7(6): 731 –742.

[18] Wang Z H, Yang B, Cheng L, et al. Robust adaptive dead zone compensation of DC servo system [J]. Control Theory and Applications, IEE Proceedings, 2006, 153(6): 709 –713.

(**Edited by** Jianying Cai)